DOI: 10.1002/chem.200500067

Synthesis, Photophysics, and Photoresponse of Fullerene-Based Azoaromatic Dyads

Giorgia Possamai,[a] Silvia Marcuz,[a] Michele Maggini,*[a] Enzo Menna,[a] Lorenzo Franco,[a] Marco Ruzzi,[a] Stefano Ceola,[a] Carlo Corvaja,[a] Giovanni Ridolfi,[b] Alessandro Geri,[b] Nadia Camaioni,[b] Dirk M. Guldi,[c] Ruediger Sens,[d] and Thomas Gessner[d]

Abstract: The synthesis and photophysical characterization of a series of fullerene-based, donor–acceptor dyads is presented, along with a description of their behavior as single molecular components in photovoltaic cells. The spectroscopic and photophysical properties of the dyads, investigated by steady-state fluorescence spectroscopy, pico- and nanosecond transient optical spectroscopy and time-resolved electron paramagnetic resonance (EPR) spectroscopy, revealed that the dyads undergo multiple-step energy transfer from the donor singlet excited state to the fullerene triplet excited state, which in turn decays to the donor triplet state. The inefficient formation of a charge-separated state, both in solution and in the solid state, translates into a poor photovoltaic performance of dyads **2b–4b** if compared to that of dyad **1b**, in which photoinduced electron transfer is operative in the solid state. In addition, the results of the photophysical investigation suggested that the performance of the solar cells was also limited by the low-lying donor triplet excited state that acts as a photoexcitation energy sink.

Keywords: donor–acceptor systems · energy transfer · EPR spectroscopy · fullerenes · solar cells

Introduction

Solar energy conversion based on organic materials is becoming an important research field with substantial future perspectives.[1–3] One of the goals of the research is the development of low-cost, large-area solar cells with good efficiency and stability in the next few years.[4] Currently, several concepts and device technologies are under intense investigation.[5] They include conjugated polymer solar cells[6] and hybrid systems, such as polymer nanocrystals[7–9] or polymer metal oxide devices.[6,10] The understanding of photoinduced processes in organic and hybrid materials coupled to the optimization of device processing has led to a substantial improvement of cell performance. In the last decade, prototype polymer solar cells, exploiting a dual molecule approach[11–13] and the bulk heterojunction principle,[14] showed solar power conversion efficiencies that triggered a renewed interest in the field. The dual molecule approach takes advantage of a second component (an electron acceptor, A) to overcome the limitation of the poor ability of conjugated polymers (acting as electron donors, D) to generate charge from light absorption. On the other hand, the bulk heterojunction principle overcomes the limitation of charge generation at a two-dimensional interface through the generation of a three-dimensional network of D–A interfaces by promoting a homogeneous distribution of the A component into the D polymer matrix. Currently, the best conjugated polymer-based solar cells reported in the literature are obtained by mixing poly(3-hexyl)thiophene and a soluble functionalized

[a] Dr. G. Possamai, Dr. S. Marcuz, Prof. M. Maggini, Dr. E. Menna, Dr. L. Franco, Dr. M. Ruzzi, Dr. S. Ceola, Prof. C. Corvaja
Dipartimento di Scienze Chimiche
Università di Padova
Via Marzolo 1, 35131 Padova (Italy)
Fax: (+39) 049-827-5239
E-mail: michele.maggini@unipd.it

[b] Dr. G. Ridolfi, A. Geri, Dr. N. Camaioni
Istituto CNR-ISOF
Via P. Gobetti 101, 40129 Bologna (Italy)

[c] Prof. D. M. Guldi
Institut für Physikalische und Theoretische Chemie
Universität Erlangen-Nürnberg
Egerlandstr. 3, 91058 Erlangen (Germany)

[d] Dr. R. Sens, Dr. T. Gessner
BASF-AG, Ludwigshafen (Germany)

Supporting information for this article is available on the WWW under http://www.chemeurj.org/ or from the author.

fullerene; these cells give a 3.5% power conversion efficiency under white light illumination and an external quantum efficiency of 70% at the absorption maximum.[15,16] It has been predicted that further improvements in the efficiencies can be achieved with conjugated polymer-based cells by optimizing the cell architecture to promote efficient exciton dissociation[17] and charge-carrier transport, and by enhancing the absorption of a larger fraction of the solar spectrum by reducing the band gap of the polymer or by using suitable chromophoric units in the blend.[2,6]

Parallel to the blend approach, the development of fullerene and conjugated polymer organic functionalization has enabled several groups to pursue alternative directions to enforce the spatial distribution of the D–A components in the solid state, thus minimizing the detrimental fullerene–polymer phase segregation frequently present in the blends.[18] Experiments to date have examined a number of so-called "double-cable" structures,[19,20] in which a functionalized fullerene is appended to a π-conjugated polymer. However, we have yet to see a fully optimized version of the double-cable device with efficiencies comparable to that reported for the blends. Other promising approaches include the use of molecular dyads and triads made of a functionalized fullerene covalently linked to oligomeric, conjugated architectures.[21–25] Such cells gave power conversion efficiencies ranging from approximately 0.02% to our recently reported 0.37%, under 80 mW cm^{-2} white light illumination, for the fullerene–azothiophene dyad[26] **1b**. The significant absorption of the dyad in the visible spectral region (λ_{max} = 567 nm), coupled to the optimization of the active layer thickness, contributed to the photovoltaic performance of cells made of dyad **1b**.

Here we report the synthesis, photoexcited state dynamics, and photovoltaic performance of three new fullerene-based azoaromatic dyads **2b**–**4b**, as an extension of our ongoing research on donor-linked fullerenes for photovoltaic applications. The photophysical behavior of the dyads, investigated by steady-state fluorescence spectroscopy, pico- and nanosecond transient optical spectroscopy, and time-resolved EPR spectroscopy, revealed that the dyads undergo multiple-step energy transfer from the dye singlet excited state to the fullerene triplet excited state, which in turn decays to the dye triplet state. The inefficient formation of a charge-separated state, both in solution and in the solid state, translates into a poor photovoltaic performance of dyads **2b**–**4b** if compared to that of dyad **1b**, in which photoinduced charge transfer is followed by charge-hopping to neighboring molecules in the solid state.

Results and Discussion

Synthesis of the fullerene–chromophore conjugates: Dyads **1b**,[26] **1d**,[27] and **2b**–**4b** are fulleropyrrolidines that were prepared through the 1,3-dipolar cycloaddition of the azomethine ylide[28] that forms when each of the (*E*)-azoaromatic aldehydes **2a**–**3a** and **6** is treated with *N*-(3,6,9-trioxadecyl)glycine[29] (or *N*-methylglycine in the case of dyad **1d**) in the presence of C_{60} in refluxing chlorobenzene. Dyads **2b**

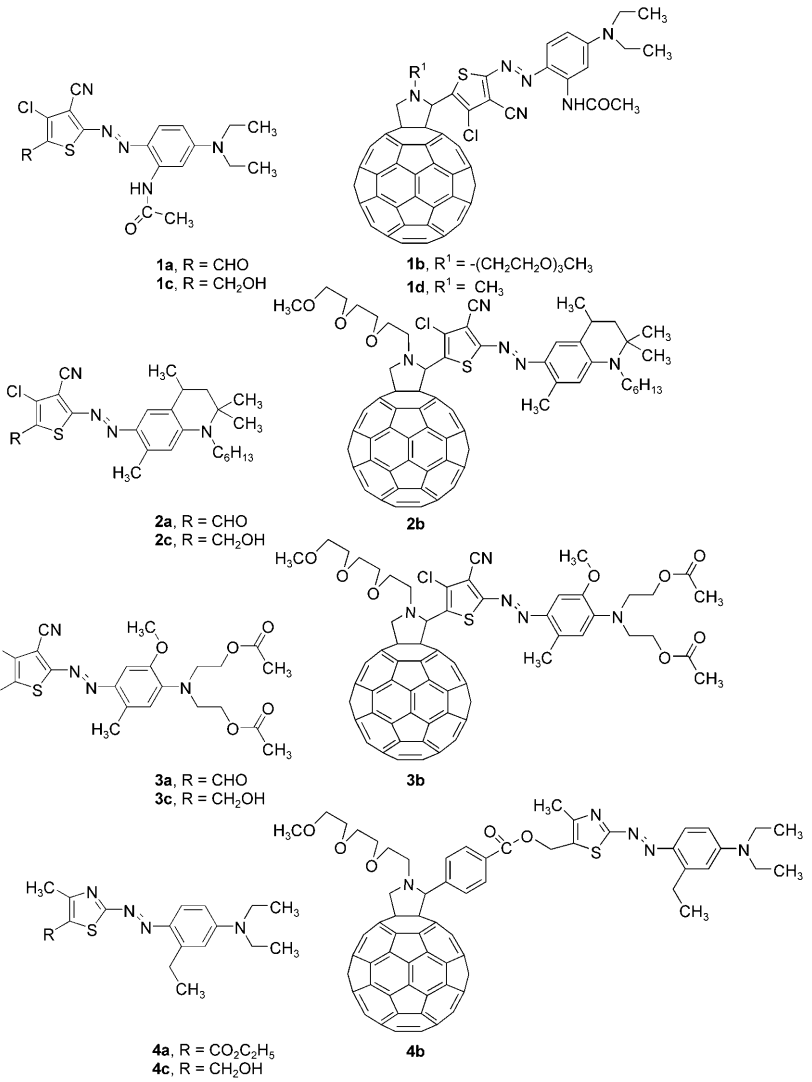

and **3b** were prepared in a single step from the corresponding azoaromatic aldehydes **2a** and **3a** in 40–45% isolated yields (Scheme 1).

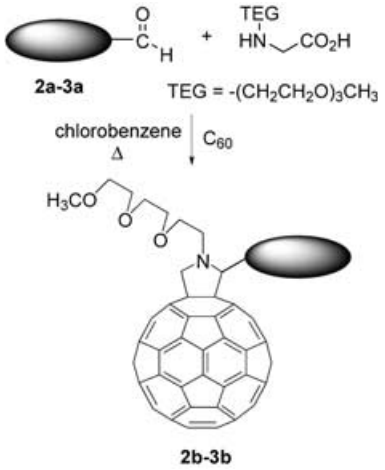

Scheme 1. Preparation of dyads **2b** and **3b** through azomethine ylide cycloaddition to C_{60}.

Dyad **4b** was prepared from aldehyde **5**, which in turn was obtained in 32% yield upon esterification of 4-carboxybenzaldehyde with the alcohol **4c** in the presence of 1-(3-dimethylaminopropyl)-3-ethylcarbodiimide (EDC). Reduction of the azoaromatic ester **4a** with $LiAlH_4$ gave alcohol **4c** in 59% yield (Scheme 2).

We used 4-carboxybenzaldehyde after several unsuccessful attempts of direct oxidation of alcohol **4c** to the corresponding aldehyde. It should be noted that aldehyde **5** was thermally unstable which caused its substantial degradation during azomethine ylide formation, and resulted in a low yield of dyad **4b**. Model alcohols **2c** and **3c** were prepared by reduction of aldehydes **2a** and **3a** with $NaBH_4$.

Photophysical measurements: The photophysical behavior of dyad **1d**, which differs from dyad **1b** only in the oxyethylene chain at the pyrrolidine nitrogen atom, was studied earlier by some of us.[27] We found that both intramolecular energy and electron transfer from the dye moiety to the fullerene core are thermodynamically feasible processes. Steady-state luminescence of **1d** in polar solvents showed a quenching of the dye singlet excited state and evidence of the fullerene singlet excited state emission. Flash-photolytic experiments, on the other hand, exhibited characteristic differential absorption changes attributed to the $C_{60}^{\bullet-}$–$dye^{\bullet+}$ charge-separated state.

Absorption characterization: All the starting dyes **1a**–**4a**, as well as model alcohols **1c**–**4c**, strongly absorb visible light in the 500–600 nm range. A comparison of the UV-visible absorption spectra of dyads **1b**–**4b** with that of *N*-methylfulleropyrrolidine[30] lacking the dye moiety (not shown) and those of model dye alcohols **1c**–**4c** (Figure 1) revealed that

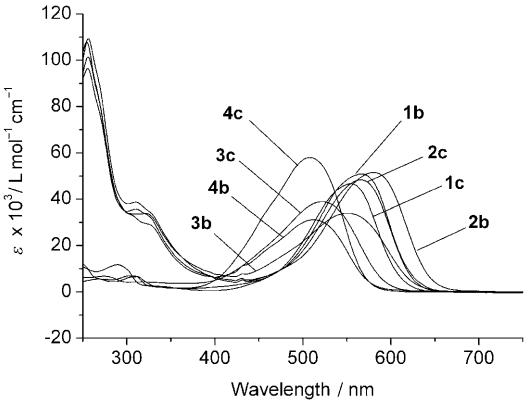

Figure 1. UV-visible absorption spectra of the dyes **1c**–**4c** and of the dyads **1b**–**4b** in CH_2Cl_2.

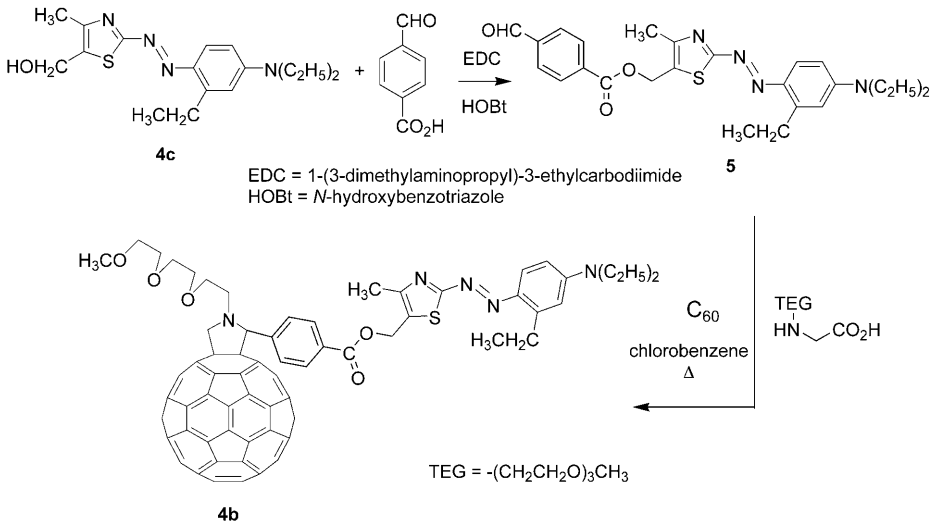

Scheme 2. Preparation of dyad **4b**.

they are mostly the superimpositions of the spectra of the components.[31]

Fluorescence characterization: Fluorescence experiments revealed information on the excited state of the individual building blocks and on the excited-state interactions between the photo- and electro-active components.

We first investigated the model dyes and the corresponding dyads in steady-state fluorescence experiments. At room temperature, the spectra of the dyes consist of a series of rather weak features, with quantum

yields of less than 10^{-4}. In the dyads, the same features are reproduced quite reasonably, but due to the overall weakness of the emissive response, a meaningful analysis was not pursued. It should be noted that the room-temperature fluorescence spectra shows the signature of the fullerene fluorescence, with a maximum at 720 nm (see Figure S1 in the Supporting Information), in a region where the dye reference does not fluoresce at all. Considering that the 500–600 nm excitation light is absorbed nearly quantitatively by the dye component, the origin of the fullerene fluorescence must be the consequence of an exothermic energy transfer between the dye and the fullerene. To confirm this assignment, we ran an independent excitation experiment monitoring the 720 nm emission as a function of excitation wavelength (see Figure S2 in the Supporting Information). This excitation survey resulted in a spectrum that closely resembles the ground-state transition of the dye component. As far as the dye's singlet excited state is concerned, the high efficiencies do not support a competitive electron-transfer scenario.

The picture changed dramatically when conducting the fluorescence experiments in a frozen matrix, such as lowering the temperature to 77 K (Figure 2).

In the dyads, the same fluorescence was quenched by factors ranging between 12 (**4b**) and 64 (**3b**). Similarly to the room-temperature studies, the fullerene reference fluoresces at around 720 nm. In the dyads, however, strong overlap with the dye fluorescence, intensities of which are comparable with those of the fullerenes, prevented any quantitative comparison (that is, quantum yield determination). Our fluorescence studies suggest that initial light irradiation in the low-energy transition of the dye (500–600 nm) is followed by a rapid singlet–singlet energy transfer. We demonstrate in the following section that the fraction of excited-state energy that is directed to the fullerene component resides there and undergoes an intersystem crossing process which is virtually identical to that found in other fullerene derivatives.

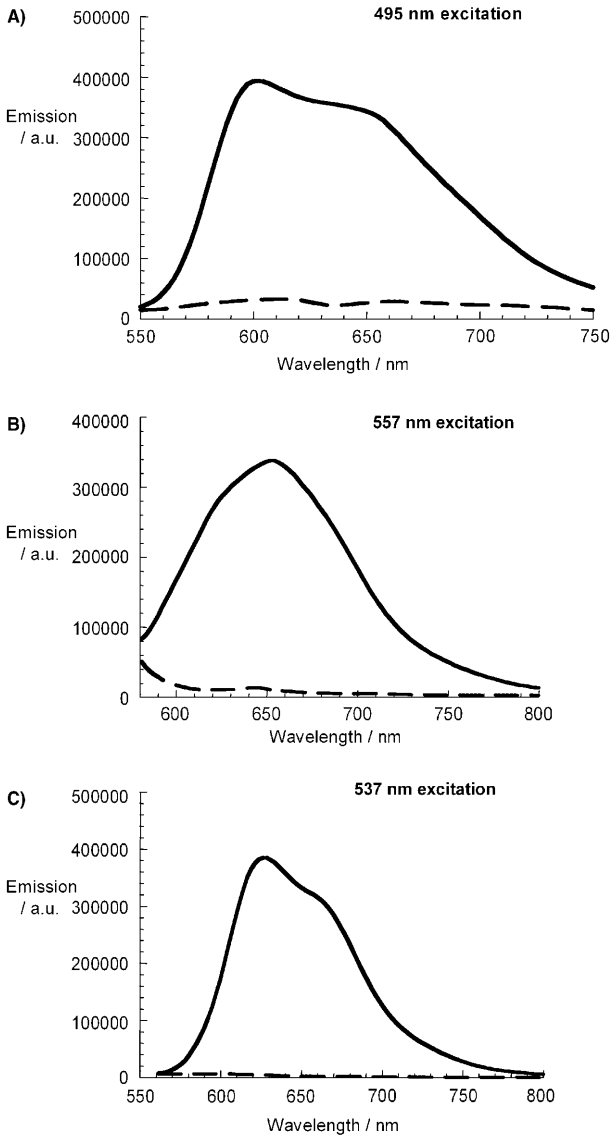

Figure 2. Low-temperature (77 K) fluorescence spectra of dyes (solid line) and dyads (dashed line) in nitrogen-saturated THF. A) **4a** and **4b** with matching absorption at 495 nm excitation wavelength; B) **3a** and **3b** with matching absorption at 537 nm excitation wavelength; C) **2a** and **2b** with matching absorption at 537 nm excitation wavelength.

Transient absorption characterization: To shed light on the nature of the product evolving from the observed intramolecular deactivation, complementary transient absorption measurements were necessary (with picosecond-through-millisecond time resolution), following the time-evolution of the characteristic singlet excited state features of the dye component.

The differential absorption changes following photoexcitation of the dyes are markedly different from those recorded for the fullerene. The photophysics of the fullerene is well known:[32] the singlet excited state of the fullerene, displaying a distinctive singlet–singlet transition around 880 nm, undergoes a quantitative intersystem crossing (ISC) with a rate of $5\times10^{8}\,s^{-1}$. The ISC process yields the long-lived triplet manifold, for which maxima are noted at 360 and 700 nm, followed by a low-energy shoulder at 800 nm.

In the differential absorption spectra of the dyes **2c**–**4c** recorded at room temperature, strong bleaching is noted in the region of the ground state absorption, namely, 450–600 nm. The bleaching, which indicates conversion of the ground state to an excited state, is flanked by a transient peak, which is located in the red region relative to the bleaching. For example, in the case of **4c** the peak maximizes at 590 nm (Figure 3).

This transient peak, which we assigned to the metastable singlet excited state (**4c**: $1.8\times10^{8}\,s^{-1}$), intersystem crosses to the long-lived triplet manifold. The latter lacks the 590 nm peak, but reveals a fairly strong transition, now blue-shifted relative to the bleaching (for example, for **4c** at 500 nm), as reported in Figure 3.

As far as the long-lived nature is concerned, we observed no clear decay over a timescale of about 200 μs for **4c** in the

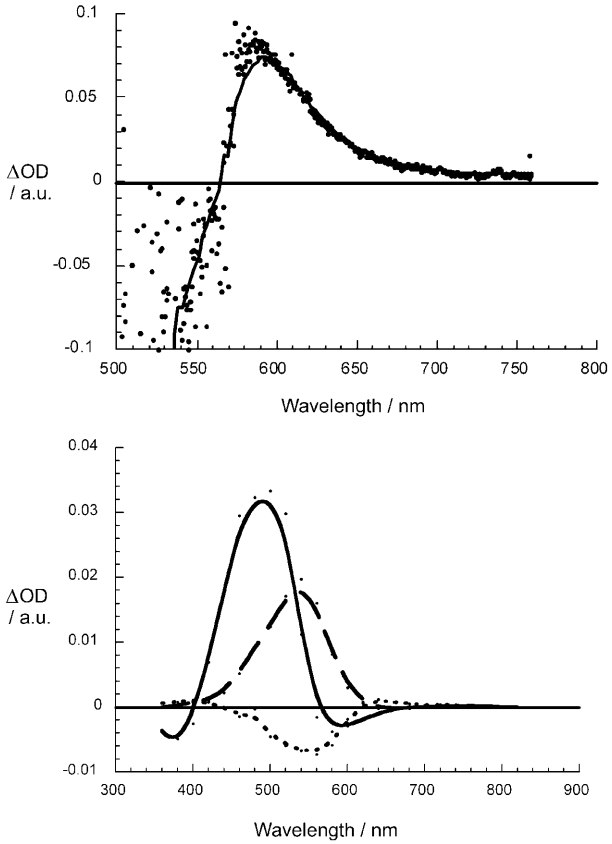

Figure 3. Differential absorption spectra obtained upon picosecond (upper panel) and nanosecond (lower panel) flash photolysis (532 nm) of nitrogen-saturated THF solutions ($\sim 1.0\times10^{-5}$ M) of **4c** (upper panel: time delay of 50 ps) indicating the singlet–singlet features of the dye, and of **2c**–**4c** (lower panel: **4c** solid line, **3c** dashed line, **2c** dotted line: time delay of 50 ns) indicating the triplet–triplet features of the dyes. Lines were obtained by fitting the experimental data points with a cubic spline option.

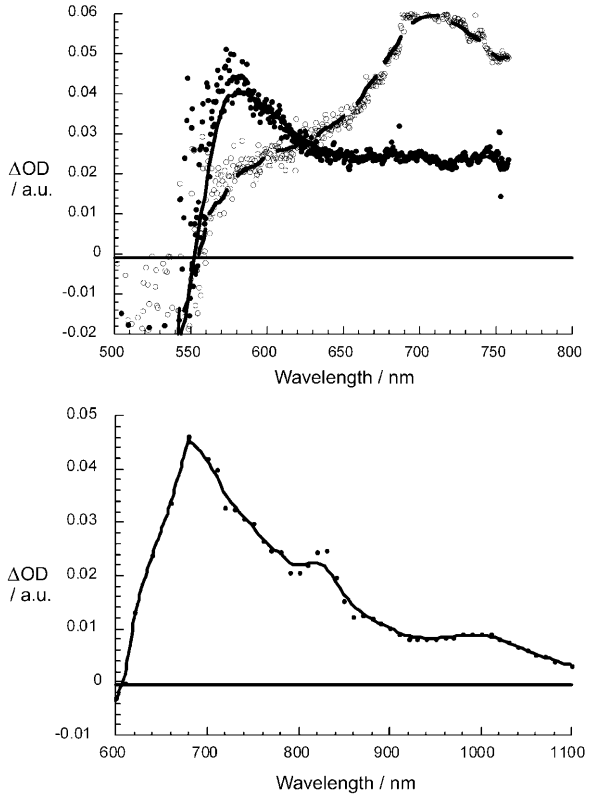

Figure 4. Upper panel: differential absorption spectra obtained upon picosecond flash photolysis (532 nm) of nitrogen-saturated THF solutions of dyad **4b** ($\sim 1.0\times10^{-5}$ M) with a time delay of 50 ps (filled circles and solid line) and 4000 ps (open circles and dashed line) indicating the singlet–singlet features of the dye and the triplet–triplet features of the fullerene respectively. Lower panel: differential absorption spectra obtained upon nanosecond flash photolysis of **4b** (same conditions as above) with a time delay of 50 ns, indicating the triplet–triplet features of the fullerene.

absence of oxygen. However, when oxygen was present, we found a nearly diffusion-controlled deactivation (see Figure S3, Supporting Information). Similar reactivities were also found for the **2c** and **3c** dyes.

Detecting the instantaneous "grow-in" of the 580 nm absorption affirms the successful dye excitation, as shown in Figure 4 for dyad **4b**.

Regarding the picosecond transient absorption measurements, immediately after the 18 ps laser excitation of the dyads **2b** and **3b**, the strong singlet–singlet absorption of the dyes was found at 650 (**2b**) and 640 nm (**3b**), similar to what is shown in Figure 4. Again this confirms, despite the presence of the fullerene, the successful formation of the dye singlet excited state. Instead of observing the slow ISC dynamics, the singlet–singlet absorption decays in the presence of the fullerene with accelerated dynamics. The dynamics reveal an interesting trend in rates: 3.7×10^{9} (**4b**) $< 4.3\times10^{9}$ (**3b**) $< 7.6\times10^{9}\ s^{-1}$ (**2b**). In other words, the stronger absorptions and emissions in the red region result in faster rates. This implies a better spectral overlap between the singlet excited state of the dye and the fullerene ground state. Parallel with decay of the dye's visible singlet–singlet transition, the formation of the fullerene singlet–singlet is discernable in the near-infrared region. For dyad **4b** we derive a formation rate of $4.0\times10^{9}\ s^{-1}$, which is in reasonable agreement with the decay rate, considering that the fullerene singlet excited state is not stable (vide infra). It is crucial to confirm the product of the dye decay as the fullerene singlet excited state, since this supports the conclusion of the fluorescence experiments, which suggested a rapid transduction of singlet-excited-state energy.

The fullerene singlet decays with conventional ISC dynamics despite the presence of the dye components. The singlet-excited-state lifetimes were determined from an average of first-order fits of the time-absorption profiles at various wavelengths (850–950 nm). For example, dyad **4b** reveals a singlet lifetime of 1.5 ns, which corresponds to an ISC rate of $6.6\times10^{8}\ s^{-1}$. Similar values emerged for **3b** and **2b**. Spectroscopically, the transient absorption changes, taken after the completion of the singlet decay, exactly resemble those with the fullerene triplet excited state. In particular, the new transients reveal strong maxima at 700 nm (Figure 4).

To examine the triplet dynamics, the dyad solutions were excited with a 6 ns laser pulse. Both maxima (360 and 700 nm) experience a similar decay, which gives rise to kinetics that obey a clean unimolecular rate-law. Surprisingly, the fullerene triplet is extremely short-lived. The longest lifetime was noted for dyad **4b**, with a value of 36 ns, as illustrated in Figure 5, which is several orders of magnitude faster than the fullerene triplet lifetime (which was 20 μs under our experimental conditions).[35]

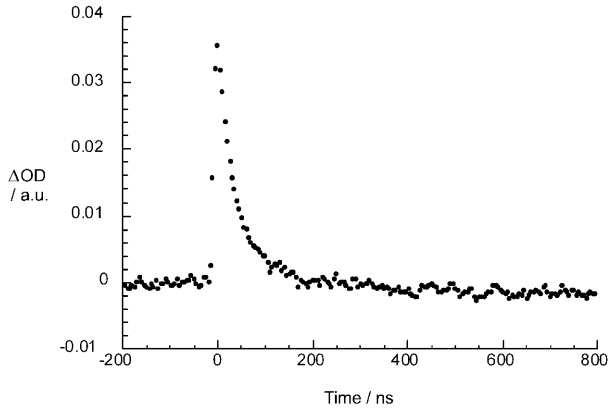

Figure 5. Time-absorption profiles at 700 nm monitoring the fullerene triplet decay dynamics of dyad **4b** in nitrogen-saturated THF.

Instead of involving the recovery of the ground state, the product of the fullerene triplet decay is the dye triplet. The shorter distance in **2b** and **3b** dyads gives rise to triplet decay dynamics faster than our instrumental response, namely, about 10 ns. This observation is in line with a triplet–triplet energy-transfer mechanism, which implies a double-electron exchange mechanism that should be distance dependent. Also in these cases, the product of the fullerene triplet decay is the dye triplet.

Interestingly, the short-lived nanosecond spectrum of the **4b** dyad reveals, in addition to the fullerene triplet, the signature of the fullerene π-radical anion, that is, a near-infrared maximum at 1000 nm. Any characteristics of the oxidized dye component are, however, masked by the strong triplet absorption. With respect to the triplet formation, we determined the contribution of the electron-transfer product as ~20%.[33] Attempts to cause higher electron-transfer yields by probing, for example, solvents of higher polarity, such as benzonitrile or DMF, were only partially successful: the major product was still the fullerene triplet. In benzonitrile the energy-to-electron-transfer ratio changed from 80:20 in THF to 70:30. Considering the fast and quantitative singlet energy transfer between the dye and the fullerene, we postulate that charge separation evolves in competition to the fullerene ISC process.

The complete photophysics of the dyads can be summarized in terms of the scheme shown in Figure 6. Light pulses photoexcite the dye unit into its excited singlet state (C_{60}–^{1}dye*).

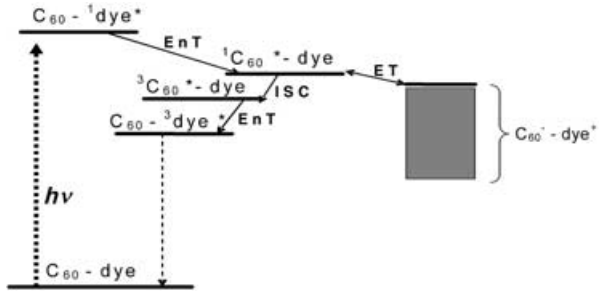

Figure 6. Schematic diagram showing the photophysics of the dyads (indicated as C_{60}–dye) after light excitation. ISC = intersystem crossing, EnT = energy transfer, ET = electron transfer. $h\nu$ = visible light photon. The energies are not drawn to scale.

A singlet–singlet energy transfer (EnT) to C_{60} is followed by ISC yielding the fullerene triplet excited state ($^3C_{60}$*–dye), which in turn decays by a second EnT step to the dye triplet excited state (C_{60}–^{3}dye*). The pathway, suggested by the transient optical absorption, is confirmed by the EPR results described below.

EPR characterization: Time-resolved EPR (TR-EPR) spectra of frozen toluene solutions of dyes **2a**–**4a** and dyads **2b**–**4b** were recorded to further investigate the dynamics of photoexcited paramagnetic states, in particular the long-lived ones. Also TR-EPR spectra of thin films of the dyads, obtained from solutions of the samples in toluene or chloroform by evaporation of the solvent, were recorded to study their solid-state photophysical properties. TR-EPR characterization of dyad **1b** both in frozen toluene and in solid film has been reported in a preliminary communication.[26] The EPR spectra of **1b** are reported here, together with those of **2b**–**4b**, for comparison. Because of the short relaxation time of triplets in liquids, EPR investigation was conducted only in frozen matrices.

Even if TR-EPR characterization is limited to long-lived states (lifetimes in the μs time range), because of the low time resolution, nevertheless the EPR spectral intensity pattern (see below) is indicative of the paramagnetic species' generation pathway, giving insight on the shorter-lived precursors and intermediates.

TR-EPR spectra of the dyes: TR-EPR spectra, extending over about 120 mT, were recorded for **1a**–**4a** at 120 K in a toluene glass-like matrix, as shown in Figure 7.

The spectra shown in Figure 7 are very similar and, as frequently occurs for photoexcited states, are spin-polarized corresponding to microwave emission at low fields and enhanced absorption at high fields. The spectra are attributed to the excited triplet states of **1a**–**4a**.

The EPR transitions of triplet state molecules are characterized by the electron–spin dipolar interaction (the zero field splitting (ZFS) interaction) between unpaired electrons and can be analyzed using the following spin Hamiltonian [Eq. (1)] in which $\boldsymbol{S}$, S_x, S_y, S_z are the electron–spin operators; g is the electron g factor; β is the Bohr magneton; $\boldsymbol{B_0}$ is

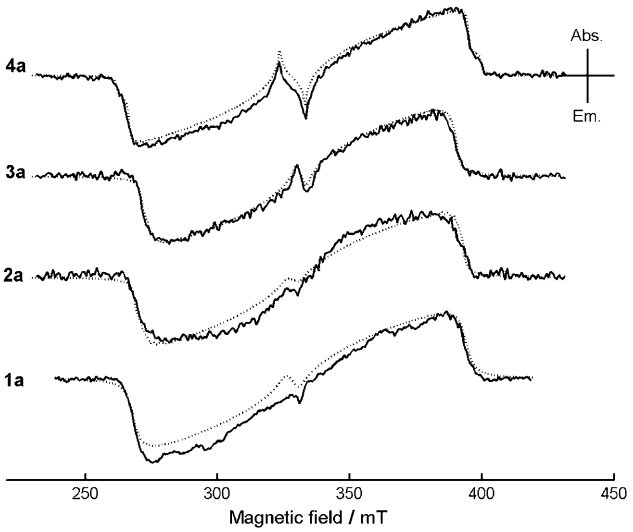

Figure 7. TR-EPR experimental spectra (solid line) and calculated spectra (dotted line) of the dyes **1a**–**4a** in frozen toluene at 120 K. The spectra are recorded 0.5 μs after the laser pulse. Abs = absorption, Em = emission.

the magnetic field intensity; D and E are parameters related to the eigenvalues X, Y, and Z of the ZFS interaction tensor [$D=3Z/2$ and $E=1/2(Y-X)$], which characterize the strength and the asymmetry of the electron dipolar coupling, respectively; and x, y, and z are the tensor principal axes.

$$H = g\beta \boldsymbol{B}_0 \boldsymbol{S} + DS_z^2 + E(S_x^2 + S_y^2) \quad (1)$$

The dye molecules in a frozen solution are randomly oriented with respect to the magnetic field direction, and the spectrum is a superposition of the signals due to all orientations. The shape of the spectrum depends critically on the relative triplet sublevel populations, determined by the selectivity of the ISC process which populates the triplet spin sublevels from the excited singlet state in a non-Boltzmann population ratio.

All spectra have been simulated using ZFS parameters (D, E) and population ratios reported in Table 1. The signs of D and E, which are not obtained from the analysis of the spectra, were assumed on the basis of simple molecular orbital calculations, which reproduce the experimental values quite well. A planar structure was assumed for the dyes, according to the geometry optimization performed at the AM1 level, and a single excited configuration HOMO–LUMO was considered for the triplet state, the frontier molecular orbitals being those calculated at the Hartree–Fock (HF) 6–31G level on the optimized geometry. The electron dipolar coupling was calculated by the point dipole approximation. It should be noted that a good fitting of the experimental spectra could be achieved even with a positive D value. In this case, contrary to that reported in Table 1, only one level should be populated, instead of two. In any case, we stress that, whatever the sign of the ZFS parameters, the EPR polarization pattern of the dye triplet state, generated by ISC from the dye excited singlet, is emission at low field and absorption at high field.

Table 1. Zero-field splitting parameters (D, E) and initial population ratios for the triplet states of dyes **1a**–**4a** obtained from simulation of TR-EPR spectra recorded 0.5 μs after the laser pulse at $T=120$ K in frozen toluene.

	D [$\times 10^{-4}$ cm^{-1}]	E [$\times 10^{-4}$ cm^{-1}]	P_x:P_y:P_z
1a	−603	−187	0.0:1.0:1.0
2a	−582	−180	0.0:0.8:1.0
3a	−561	−173	0.0:1.0:1.0
4a	−645	−185	0.0:0.9:1.0

TR-EPR spectra of the dyads: The TR-EPR spectra of the dyads **1b**–**4b**, recorded in frozen toluene, are markedly different from the spectra of the dyes, as shown in Figure 8.

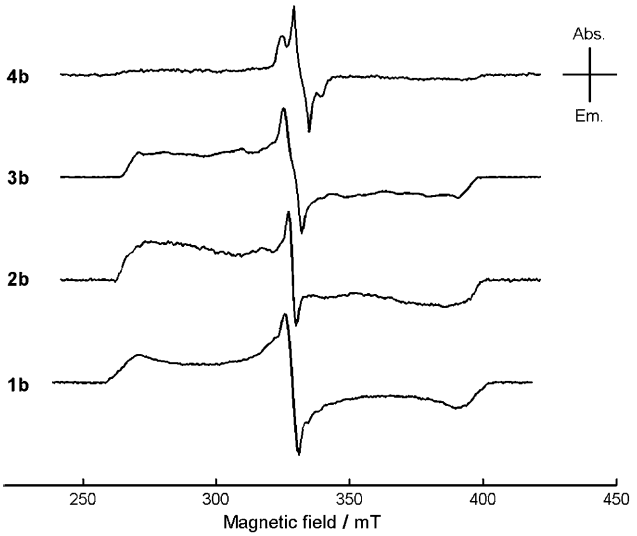

Figure 8. TR-EPR experimental spectra of the dyads **1b**–**4b** in frozen toluene at 120 K. The spectra are recorded 0.5 μs after the laser pulse. Abs = absorption, Em = emission.

The spectral width corresponds to that of the dyes (150 mT), but the polarization pattern is inverted: absorption at low field and emission at high field. This pattern is the same as that obtained with *N*-methylfulleropyrrolidine and several other C_{60} monoadducts in the photoexcited triplet state.[34] Moreover, the features in the center of the spectrum are much more pronounced.

The absorption/emission pattern can be understood if we consider that in the dyads the spin selectivity is governed by the fullerene properties, since ISC takes place in the $^1C_{60}$*–dye state (see Figure 6). The dye triplet in this case is formed by a spin-conserving triplet–triplet (T–T) energy transfer[35] from the fullerene unit to the dye moiety. The population of the zero-field eigenstates of the energy acceptor (P_j^{EA}) can be calculated from the zero-field triplet population of the energy-donor (P_i^{ED}) by projecting the principal directions of the donor onto the principal directions of

the acceptor, once the mutual orientation is known.[36,37] Using the optimized geometries of the dyes, the calculated principal directions for each dye triplet, and the principal directions of the fulleropyrrolidine,[38] we obtained population ratios for the dyes that reasonably reproduce those determined experimentally.

For dyads **1b–3b**, the T–T energy transfer occurs in a shorter time than the TR-EPR timescale. As a consequence, the TR-EPR spectrum recorded after photoexcitation of the dyads is that of the azo-dye triplet, but reminiscent of the population pattern generated by the ISC on C_{60}. Conversely, the T–T energy transfer in **4b** is slower, with a rate constant of about 0.9 μs. This result agrees with the transient absorption measurements, which evidenced slower kinetics of the triplet–triplet energy transfer in the **4b** dyad, caused by the longer distance between the triplet donor (the fullerene) and the triplet acceptor (the dye unit).

TR-EPR spectra on films: All the previous photophysical investigations on dyads **1b–4b** were performed in dilute solutions. On the other hand, the solar cells described in the next section are solid-state devices in which the active component is an aggregated thin film. For this reason, we also examined TR-EPR spectra of dyad films produced by evaporation of solutions of the dyad in toluene or chloroform. The spectra are quite different from those taken in frozen toluene; instead of a broad lineshape with alternate polarization attributed to localized triplet states, only relatively narrow lines in emission are obtained for films of dyads **1b–4b** (Figure 9).

For dyad **1b**, a narrower line in absorption, superimposed onto a wider line in emission, is also visible. The narrow line g factor ($g = 2.0005 \pm 0.0005$) could be reasonably attributed to the fullerene radical anion.[39] This demonstrates that an electron transfer takes place after light excitation, and that the charge-separated state is sufficiently long-lived (about 1 μs) to be detected. On the other hand, for dyads **2b–4b** the line in absorption is missing (or extremely weak), indicating the absence of a long-lived charge-separated state. In contrast, the emissive line intensity increases, being very strong for dyad **4b** (Figure 9).

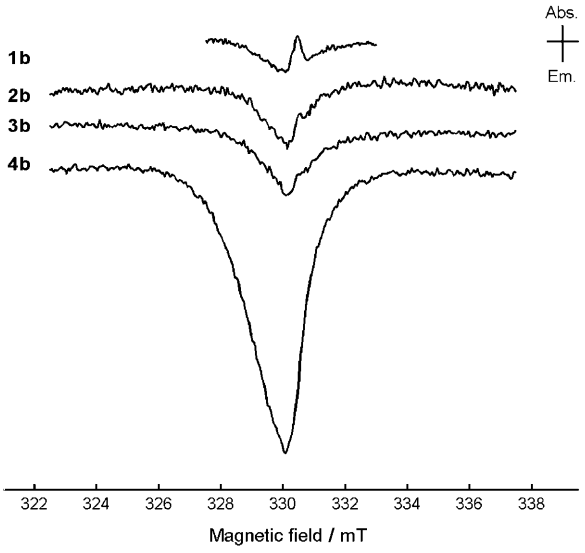

Figure 9. TR-EPR spectra of film of dyads **1b–4b**, recorded 0.5 μs after the laser pulse, at 140 K. Abs = absorption, Em = emission.

In the dyads **2b–4b**, photoinduced electron transfer from the dye to the fullerene is not revealed by TR-EPR spectroscopy. This fact does not exclude the formation of charge carriers. These might not be spin-polarized and therefore undetectable by TR-EPR spectroscopy, or may be too short-lived due to back-electron transfer faster than the TR-EPR instrumental time resolution (about 150 ns).

Photovoltaic devices: Photocells were prepared with comparable thickness (80–90 nm) of the active layer. The photovoltaic cells, prepared under ambient conditions apart from the cathode deposition, were tested in vacuum (10^{-3} mbar) under white light irradiation of about 80 mW cm^{-2}. The current–voltage characteristics of cells made from films of dyads **1b–4b** are shown in Figure 10, whereas the related photovoltaic parameters are shown in Table 2. It should be noted that the photovoltaic parameters of photocells with dyad **1b**, listed in Table 2 for a better comparison, have already been reported.[26]

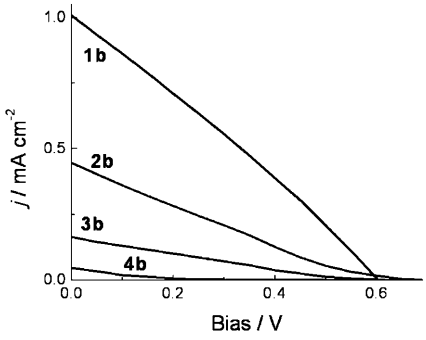

Figure 10. Current–voltage curves of cells made from dyads **1b–4b**. White light irradiation power: 80 mW cm^{-2}. Active layer thickness: 80–90 nm. Room temperature.

Table 2. Solar cell photovoltaic parameters under 80 mW cm^{-2} white light irradiation. Active-layer thickness: 80–90 nm. Room temperature.

	j_{SC} [A cm^{-2}][a]	V_{OC} [V][b]	FF[c]	η [%][d]
1b	1.0×10^{-3}	0.60	0.28	2.1×10^{-1}
2b	4.5×10^{-4}	0.70	0.20	7.9×10^{-2}
3b	1.7×10^{-4}	0.61	0.22	2.9×10^{-2}
4b	4.6×10^{-5}	0.39	0.11	2.4×10^{-3}

[a] j_{sc}: short-circuit current density. [b] V_{oc}: open-circuit voltage. [c] FF: fill factor. [d] η: power conversion efficiency.

The different values of the open-circuit voltage (V_{oc}) could be justified either by different energetics of the materials, as it occurs in the case of polymer–fullerene-blended devices,[40] or by different shunt effects. Rather low values

for the fill factor (FF), ranging between 0.28 and 0.11, were calculated for the investigated cells. It is worth noting that the FF reported so far for fullerene-based double-cable or D–A dyad solar cells[22,24,41,42] are quite low, if compared with those usually published for blended cells.[15] In general, an increasing series resistance and a decreasing shunt resistance tend to reduce the fill factor, although other factors related to the diode properties and/or the material transport properties, cannot be ruled out.

The best photovoltaic performance was achieved with cells made of dyad **1b**, with a short-circuit current (j_{sc}) of 1.0 mA cm^{-2} and a power conversion efficiency (η) of 0.21 %. The cells based on the other dyads exhibited decreased efficiencies, showing a reduction of η of two orders of magnitude for **4b**-based devices (2.4×10^{-3} %).

In this last case, the reduced V_{OC} (0.39 V) and FF (0.11) values, with respect to V_{OC} and FF of cells made of the other dyads, contributed to the poor conversion efficiency. However, the variation of the short-circuit current of more than one order of magnitude (from 1.0×10^{-3} to 4.6×10^{-5} A cm^{-2}), leading to the remarkable variation of η, is hardly justifiable on the basis of differences of the active-layer optical density. Active layers **1b** and **2b** did not display different capability of light absorption, whereas a loss of only 40 or 50 % was observed for the absorbance of **3b** and **4b** films, respectively (Figure 11). Therefore different transport properties and/or carrier photogeneration capabilities of the three active layers could be hypothesized.

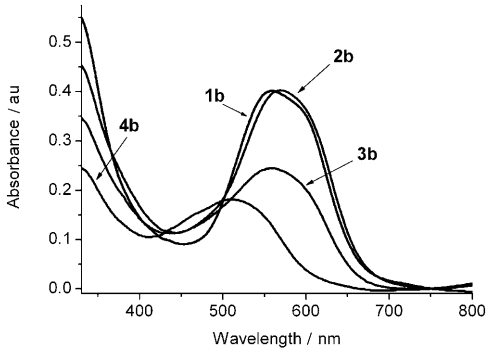

Figure 11. Absorption spectra of films of dyads **1b**–**4b**. The films, 80–90 nm thick, were spin-coated from chloroform onto glass–ITO substrates.

The charge-carrier generation and mobility in the active layer depend on the structure and supramolecular organization in the solid state of the specific dyad under investigation. Recently, it has been shown that both hole and electron mobility of a series of fullerene–oligophenyleneethynylene compounds are strongly dependent on the oligomer chain length.[43] Given the molecular structures of the three dyads investigated here, meaningful differences in the transport properties are not expected on the basis of their chemical structure.

To analyze the active-layer morphology, scanning force microscopy (SFM) imaging in the noncontact mode was performed on films made from the four different dyads. The investigated thin films, with a thickness of about 90 nm, were spin-coated onto ITO-covered glass substrates previously covered by an 80 nm layer of PEDOT/PSS (PEDOT/PSS poly(3,4-ethylenedioxythiophene) doped with polystyrene sulfonic acid; from Bayer AG). No meaningful differences were observed in the morphology of the four active layers. A representative SFM image is shown in Figure 12, in which the film-forming properties of dyad **2b** are displayed.

The image reveals a fairly smooth surface which exhibits

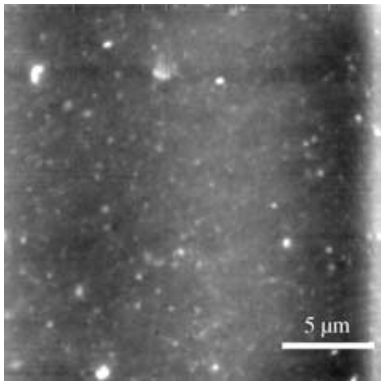

Figure 12. Topographical SFM image, recorded in non-contact mode, of a dyad **2b** film. The film, approximately 90 nm thick, was deposited onto an ITO substrate previously coated with a 80 nm thick layer of PEDOT:PSS. Z-scale: 20 nm.

some taller grains with a diameter up to some hundreds of nanometers and height of 10–50 nm. Since the investigated active layers lack of any supramolecular order, under the deposition conditions and in the investigated scale, it is reasonable to assume them to be amorphous, in agreement with the results of a study reported earlier on films of dyad **1b**.[44]

Different carrier photogeneration capabilities of dyads **1b**–**4b** could account for the different photovoltaic performance. It is interesting to note that the intensity of the TR-EPR anion line (Figure 9) correlates with photovoltaic efficiency: the highest performance is achieved with **1b**, which has the stronger anion signal. In contrast, solar cells made of dyads **2b**–**4b** display a very poor efficiency, with **4b** being the most inefficient.

Conclusion

We have shown that a series of structurally similar donor-linked fullerenes (**1b**–**4b**) give rise to very different photovoltaic performance when used as active components in solar cells. A first justification for this behavior came from a photophysical study in solution, which revealed multiple-step energy-transfer processes for all investigated com-

pounds. Only electron transfer for dyads **1b** and **4b**, necessary for photovoltaic solar cell operation,[14] evolves in competition with energy transfer. However, a TR-EPR study carried out on films of dyads **1b**–**4b** obtained from solutions of the dyads in toluene, revealed that only dyad **1b** showed transient spectra with a narrow absorption line, the *g* factor and linewidth of which were typical of radical anions of fullerene derivatives. On the other hand, dyads **2b**–**4b** showed transient EPR spectra with no lines in absorption but showed an emissive line, of increasing intensity from **2b** through **4b**, that has been attributed to local defects in the material acting as energy or charge traps. This is illustrated in Figure 6 by the lowest energy levels of the charge-separated state (C_{60}^{-}–dye^{+}). The increased intensity of the emissive line from **2b** through **4b** correlates well with decreased efficiencies exhibited by solar cells based on dyad **2b** (7.9×10^{-2}%), **3b** (2.9×10^{-2}%), and **4b** (2.4×10^{-3}%). In particular, the higher conformational freedom between the fullerene and dye units in **4b**, if compared to that of dyads **2b** and **3b**, probably favors the formation of more efficient traps in the film that are detrimental for charge transport and collection at the electrodes in a solar cell. Although a comprehensive understanding of the relation amongst molecular structure, morphology, and device performance[45] is still lacking for solar cells based on a single D–A component, we have shown that TR-EPR spectroscopy emerged as a valuable tool for a rapid screening of the electron-transfer characteristics of functionalized fullerenes in the solid state for photovoltaic conversion. In addition, the results of the photophysical investigation reported above suggest that the performance of solar cells made of donor-linked fullerenes could be enhanced if the triplet excited state of the donor structure is not placed too low in energy, if compared to the fullerene triplet, to act as a photoexcitation energy sink.

Experimental Section

Photophysics: Absorption spectra were recorded with a Perkin–Elmer Lambda 5 spectrophotometer. Emission spectra were recorded on a SLM 8100 Spectrofluorimeter. Fluorescence spectra were measured at liquid nitrogen or room temperature. A 500 nm long-pass filter was used in the emission path in order to eliminate the interference from the solvent and stray light. Long integration times (20 s) and low increments (0.1 nm) were applied. The slits were 2 and 8 nm wide. Each spectrum was an average of at least five individual scans. Time-resolved EPR measurements were carried out with a Bruker ER200D spectrometer equipped with a broadband preamplifier (6.5 MHz) in direct detection mode, that is, without magnetic-field modulation and lock-in amplification. The transient signal was recorded with a LeCroy LT344 digital oscilloscope. The optical excitation was obtained with a frequency-doubled Nd–YAG laser (Quantel Brilliant, $\lambda=532$ nm, pulse-length 5 ns, repetition rate 20 Hz, pulse energy 5 mJ). The sample temperature was controlled in the 100–300 K range by a variable-temperature nitrogen flow system (Bruker ER4112 VT). EPR samples in toluene solutions ($\sim10^{-4}$ M) were degassed by repeated freeze-pump-thaw cycles and sealed under vacuum in 4 mm (outer diameter) quartz tubes. Dyad films were obtained by evaporation of solutions of the dyads in toluene or chloroform inside the EPR tubes under vacuum.

Photovoltaic devices: The device photoactive layers were spin-coated (2000–3000 rpm) from solutions of the samples in chloroform (15 g L^{-1}) onto indium-tin-oxide (ITO) glass substrates previously coated with a layer of PEDOT/PSS. The film thicknesses were routinely determined by using a profilometer Alpha Step 200 (Tencor Instruments). The absorption spectra of the active layers were taken with a Perkin–Elmer λ9 spectrophotometer. Photovoltaic devices were prepared by subliming an aluminum top electrode in vacuum. The active area of the devices was 3.14 mm^2. Except for the cathode deposition, each step of the device fabrication was performed in ambient conditions. The electrical characterization of the devices was done with a Keithley 2400 source-measure unit, under a pressure of 10^{-3} mbar and at room temperature. The junctions were illuminated through the ITO side with a 300 W Xe arc lamp. The intensity of the incident light, measured with an Oriel thermopile, was about 80 mW cm^{-2}. The optical bench was equipped with a water filter to cut off IR radiation. No correction was made for light reflection.

Microscopy: Noncontact scanning force microscopy[46] was employed for recording both the height signal (output of the feedback signal) and the phase signal (phase lag of the oscillation relative to the driver). While the first type of image provides a topographical map of the surface, the latter is extremely sensitive to structural heterogeneities on the sample surface, and therefore ideal to identify different components in a hybrid film. The SFM Autoprobe CP Research thermomicroscope was operated in air at room temperature with scan rates of 1 Hz per line. Images with scan lengths ranging from 30 μm down to 5 μm were recorded with a resolution of 512×512 pixels using the 100 μm scanner and noncontact Si ultralevers with a spring constant of $k=2.1$ N m^{-1}.

General remarks and materials: Details regarding the instrumentation used in this work to characterize all new compounds have been described elsewhere.[47] The mass spectra were recorded on a Mariner ESI-TOF mass spectrometer (Perspectives Biosystems). C_{60} was purchased from Bucky (USA)(99.5% purity). *N*-(3,6,9-Trioxadecyl)glycine,[29] dyad **1b**,[26] alcohol **1c**,[27] dye aldehydes **2a** and **3a**, and ester **4a** were prepared as previously reported.[48] All other reagents were used as purchased from Aldrich. The solvents for UV-visible, steady-state luminescence, pico- and nanosecond flash photolysis and EPR measurements were commercial spectrophotometric-grade solvents that were carefully deoxygenated prior to use.

General experimental procedure for the synthesis of dyads 2b–4b: C_{60} (1 equiv), *N*-(3,6,9-trioxadecyl)glycine (2 equiv), and the appropriate dye aldehyde (1 equiv) were dissolved in chlorobenzene (50 mL per 100 mg of C_{60}) and brought to reflux temperature. The reaction was monitored by TLC (SiO_2, see below for further details) and was stopped just after the formation of traces of multiple adducts to C_{60}; these adducts were detectable by TLC and had a lower retention factor than the dyad monoadduct. The crude mixture, loaded onto a SiO_2 flash column for chromatography, was first eluted with toluene to remove unreacted C_{60} and then with toluene/ethyl acetate mixtures (vide infra). The fractions containing the product were concentrated to a small volume under reduced pressure and were transferred into a centrifuge tube. The product was precipitated from acetonitrile, washed twice with the same solvent and was dried under reduced pressure.

Dyad 2b: Reagents: C_{60} (80 mg, 0.1 mmol), *N*-(3,6,9-trioxadecyl)glycine (40 mg, 0.2 mmol), aldehyde **2a** (52 mg, 0.1 mmol) in chlorobenzene (100 mL). Reaction time: 40 min. TLC: toluene/ethyl acetate 9:1, R_f (**2b**) = 0.27). Flash column chromatography: toluene/ethyl acetate 9:1; 66 mg (44% yield). ^{1}H NMR (250 MHz, $CDCl_3$): $\delta=7.82$ (s, 1H), 6.36 (s, 1H), 5.79 (s, 1H), 5.20 (d, 1H), 4.39 (d, 1H), 3.75 (m, 8H), 3.56 (m, 4H), 3.36 (s, 3H), 3.05 (m, 1H), 2.83 (m, 1H), 2.61 (s, 3H), 1.58 (m, 4H), 1.38 (m, 15H), 1.25 (d, 4H), 0.93 ppm (3H); ^{13}C NMR (62.9 MHz, $CDCl_3$): $\delta=169.17$, 155.92, 153.66, 152.98, 150.85, 147.31, 146.25, 146.21, 146.18, 146.13, 146.01, 145.64, 144.60, 144.40, 144.33, 143.05, 14.98, 142.11, 140.76, 140.16, 139.95, 137.60, 136.49, 135.59, 135.53 , 132.96, 129.01, 128.20, 127.50, 125.28, 113.19, 112.52, 72.00, 70.74, 70.69, 70.17, 69.17, 67.63, 56.23, 56.18, 52.59, 45.59, 31.41, 29.49, 26.80, 22.60, 26.77, 19.75, 18.29, 13.99 ppm; IR (KBr): $\tilde{\nu}=3432$, 2923, 2221, 1601, 1526, 1504, 1461, 1308, 1281, 1239, 1186, 1221, 1121, 1054, 1016, 901, 727, 703, 573, 525 cm^{-1}; UV/Vis (CH_2Cl_2): $\lambda_{max}(\varepsilon)=200.8$ (45860), 228.8 (91535), 256.0 (109360),

310.4 (38640), 431.2 (5155), 580.8 nm (51475 $mol^{-1}dm^3cm^{-1}$); MS (ESI-TOF): *m/z* 1352 [M^+]; elemental analysis calcd (%) for $C_{93}H_{48}ClN_5O_3S$ (1350.93): C 82.68, H 3.58, N 5.18, S 2.37; found: C 82.11, H 3.23, N 5.00, S 2.38.

Dyad 3b: Reagents: C_{60} (80 mg, 0.1 mmol), *N*-(3,6,9-trioxadecyl)glycine (40 mg, 0.2 mmol), aldehyde **3a** (56 mg, 0.1 mmol) in chlorobenzene (100 mL). Reaction time: 2 h. TLC: toluene/ethyl acetate 7:3, R_f (**3b**)= 0.39. Flash column chromatography: toluene/ethyl acetate 9:1, 21 mg (43% yield). ^{1}H NMR (250 MHz, $CDCl_3$): δ=7,60 (s, 1H), 7.35 (s, 1H), 5.75 (s, 1H), 5.15 (d, 1H), 4.34 (d, 1H), 4.20 (m, 4H), 4.70–3.40 (complex system of resonances due to aliphatic protons, 18H), 3.29 (s, 4H), 2.57 (s, 3H), 1.95 ppm (s, 6H); ^{13}C NMR (62.9 MHz, $CDCl_3$): δ=170.85, 155.79, 152.74, 149.97, 147.38, 146.25, 145.55, 145.37, 145.22, 144.82, 144.79, 144.69, 144.12, 143.31, 142.57, 142.50, 142.17, 142.14, 142.09, 141.70, 141.66, 141.56, 141.47, 141.39, 141.16, 139.41, 137.16, 137.00, 135.88, 135.31, 135.09, 129.33, 129.27, 128.96, 127.32, 127.15, 126.76, 125.40, 117.93, 113.46, 99.60, 74.86, 74.60, 71.49, 70.22, 70.17, 69.57, 68.63, 67.13, 61.69, 58.57, 55.17, 52.13, 51.47, 50.98, 50.00, 29.17, 21.01, 20.34, 16.73, 10.30 ppm; IR (KBr): $\tilde{\nu}$=3434, 2918, 2850, 2224, 1739, 1592, 1505, 1461, 1372, 1320, 1222, 1185, 1138, 1102, 1043, 765, 696, 596, 573, 561, 552, 525 cm^{-1}; UV/Vis (CH_2Cl_2): $\lambda_{max}(\varepsilon)$=201.6 (43825), 228.8 (87345), 256.0 (101375), 321.6 (33825), 431.2 (7760), 551.2 nm (33985 $mol^{-1}dm^3cm^{-1}$); MS (ESI-TOF): *m/z*: 1387 [M^+]; elemental analysis calcd (%) for $C_{90}H_{40}ClN_5O_8S$ (1386.83): C 77.95, H 2.91, N 5.05, S 2.31; found: C 76.90, H 3.09, N 4.63, S 2.15.

Dyad 4b: Reagents: C_{60} (80 mg, 0.1 mmol), *N*-(3,6,9-trioxadecyl)glycine (40 mg, 0.2 mmol), aldehyde **5** (50 mg, 0.1 mmol) in chlorobenzene (80 mL). Reaction time: 2.5 h. TLC: toluene/ethyl acetate 9:1, R_f (**4b**)= 0.35. Flash column chromatography: toluene to recover unreacted C_{60} (66 mg, 83%) then toluene/ethyl acetate 9:1; 11 mg (8% yield). ^{1}H NMR (250 MHz, $CDCl_3$): δ=8.10 (d, 2H), 7.94 (d, 2H), 6.54 (m, 3H), 5.45 (s, 2H), 5.23 (d, 2H), 4.32 (d, 1H), 3.75 (m, 6H), 3.47 (m, 11H), 3.03 (m, 2H), 2.55 (s, 3H), 1.24 ppm (m, 11H); ^{13}C NMR (62.9 MHz, $CDCl_3$): δ= 165.98, 156.24, 154.15, 152.99, 152.72, 152.10, 151.85, 149.90, 147.30, 146.50, 146.37, 146.30, 146.24, 146.19, 146.13, 146.08, 145.91, 145.78, 145.69, 145.54, 145.49, 145.30, 145.24, 145.18, 144.69, 144.5, 144.39, 144.34, 143.12, 142.66, 142.24, 142.07,141.97, 141.83, 141.65, 141.52, 140.15, 139.89, 136.96, 136.44, 135.93, 135.58, 130.13, 129.84, 129.56, 125.01, 124.57, 119.21, 110.45, 110.26, 81.88, 72.02, 70.76, 70.69, 70.65, 70.30, 69.27, 67.63, 59.09, 58.79, 52.10, 44.84, 32.19, 30.92, 29.68, 26.38, 25.54, 23.42, 16.85, 15.44, 12.79 ppm; IR (KBr): $\tilde{\nu}$=3440, 2964, 2922, 1719, 1595, 1543, 1509, 1455, 1350, 1243, 1178, 1107, 1074, 1018, 849, 806, 764, 703, 527 cm^{-1}; UV/Vis (CH_2Cl_2): $\lambda_{max}(\varepsilon)$=202.4 (40745), 228.8 (82615), 256.0 (96385), 512.0 nm (31140 $mol^{-1}dm^3cm^{-1}$); MS (ESI-TOF): *m/z*: 1345 [M^+].

Alcohol 2c: $NaBH_4$ (13 mg, 0.35 mmol) in ethanol (15 mL) was added dropwise to a solution of dye aldehyde **2a** (150 mg, 0.3 mmol) in ethanol (100 mL) at room temperature. When the addition was complete, the mixture was heated to reflux for 3 h. TLC: toluene/ethyl acetate 7:3, R_f (**2c**)=0.8. The solvent was evaporated under reduced pressure and the crude product purified by flash column chromatography (SiO_2). Elution with toluene/ethyl acetate 9:1 gave **2c** (85 mg, 58% yield). M.p.=152–153°C; ^{1}H NMR (250 MHz, $CDCl_3$): δ=7.81 (s, 1H), 6.35 (s, 1H), 4.78 (s, 2H), 3.36 (m, 2H), 2.54 (s, 3H), 2.85 (m, 1H), 2.09 (s, 1H), 1.74 (m, 4H), 1.55 (d, 13H), 1.26 (s, 3H), 0.94 ppm (s, 3H); ^{13}C NMR (62.9 MHz, $CDCl_3$): δ=167.76, 150.66, 142.7, 140.39, 134.63, 127.45, 121.74, 115.69, 113.15, 112.40, 105.23, 58.24, 56.12, 45.92, 45.57, 31.42, 29.50, 28.76, 26.80, 25.82, 22.63, 19.77, 17.89, 13.98 ppm; IR (KBr): $\tilde{\nu}$=3458, 2960, 2928, 2224, 1602, 1530, 1506, 1462, 1367, 1325, 1311, 1283, 1241, 1221, 1193, 1149, 1123, 1054, 903, 837, 704, 541 cm^{-1}; UV/Vis (CH_2Cl_2): $\lambda_{max}(\varepsilon)$= 206.4 (5615), 216.0 (5380), 226.4 (8380), 228.8 (8080), 301.6 (6910), 564.8 nm (48305 $mol^{-1}dm^3cm^{-1}$); elemental analysis calcd (%) for $C_{25}H_{33}ClN_4OS$ (473.07): C 63.47, H 7.03, N 11,84; found: C 63.42, H 7.19, N 11.45.

Alcohol 3c: $NaBH_4$ (4 mg, 0.01 mmol) in ethanol (5 mL) was added to a solution of dye aldehyde **3a** (50 mg, 0.01 mmol) in ethanol (50 mL) over a dry ice/acetone cooling bath under an inert atmosphere. When the addition was complete, the mixture was left at that temperature for 2 h TLC: toluene/ethyl acetate 7:3, R_f (**3c**)=0.46. The solvent was evaporated under reduced pressure and the crude product purified by flash column chromatography (SiO_2). Elution with toluene/ethyl acetate 9:1 gave **3c** (27 mg, 53% yield). M.p.=160–165°C; ^{1}H NMR (250 MHz, $CDCl_3$): δ=7.39 (m, 2H), 6.75 (s, 1H), 4.81 (d, 2H), 4.26 (t, 4H), 3.86 (s, 3H), 3.69 (t, 4H), 2.55 (d, 3H), 2.05 ppm (s, 6H); ^{13}C NMR (62.9 MHz, $CDCl_3$): δ=170.89, 165.88, 150.05, 145.10, 143.22, 137.45, 137.05, 118.68, 112.55, 99.44, 62.24, 58.34, 55.69, 51.45, 20.85, 16.87, 16.83 ppm; IR (KBr): $\tilde{\nu}$=3450, 2959, 2923, 2225, 1735, 1705, 1592, 1532, 1509, 1480, 1374, 1321, 1280, 1242, 1221, 1193, 1151, 1103, 1047, 916, 865 cm^{-1}; UV/Vis (CH_2Cl_2): $\lambda_{max}(\varepsilon)$=212.0 (14450); 273.6 (6775); 522.4 nm (38845 $mol^{-1}dm^3cm^{-1}$); elemental analysis calcd (%) for $C_{25}H_{25}ClN_4O_6S$ (545.01): C 51.92, H 4.95, N 11.01; found: C 53.07, H 5.01, N 10.20.

Alcohol 4c: $LiAlH_4$ (1.5 mL, 1M solution in THF) in THF (5 mL) was added dropwise to a solution of dye ester **4a** (500 mg, 1.34 mmol) in THF (40 mL) over a dry ice/acetone cooling bath under an inert atmosphere. When the addition was complete, the mixture was left at that temperature for 1.5 h. TLC: toluene/ethyl acetate 8:2, R_f (**4c**)=0.18. Excess $LiAlH_4$ was quenched with ethyl acetate (50 mL). The solvents were evaporated under reduced pressure and the crude product purified by flash column chromatography (SiO_2). Elution with toluene/ethyl acetate 95:5 gave **4c** (263 mg, 59% yield). M.p.=106–107°C; ^{1}H NMR (250 MHz, $CDCl_3$): δ=7.89 (d, 1H), 6.49 (m, 2H), 4.78 (s, 2H), 3.42 (quart, 4H), 2.99 (quart, 2H), 2.38 (s, 3H), 1.22 ppm (m, 9H); ^{13}C NMR (62.9 MHz, $CDCl_3$): δ=176.92, 151.81, 149.59, 148.50, 139.61, 131.43, 118.82, 110.39, 110.13, 57.05, 44.71, 25.57, 16.83, 15.11, 12.69 ppm; IR (KBr): $\tilde{\nu}$=3418, 2970, 2926, 1597, 1547, 1510, 1450, 1350, 1246, 1180, 1110, 1074, 1016, 893, 841, 805, 739 cm^{-1}; UV/Vis (CH_2Cl_2): $\lambda_{max}(\varepsilon)$= 216.0 (9650), 225.6 (11350), 228.0 (11290), 230.4 (11065), 290.4 (11740), 508.0 nm (57900 $mol^{-1}dm^3cm^{-1}$).

Aldehyde 5: *N*-Hydroxybenzotriazole hydrate (HOBt) (89 mg, 0.7 mmol), 1-(3-dimethylaminopropyl)-3-ethylcarbodiimide (EDC, 127 mg, 0.7 mmol), and *N*,*N*-dimethylaminopyridine (DMAP, 59 mg, 0.5 mmol) were added to a solution of 4-carboxybenzaldehyde (90 mg, 0.6 mmol) in CH_2Cl_2 (40 mL), and the flask was immersed in an ice bath. Dye alcohol **4c** (200 mg, 0.6 mmol) was added, the ice-bath was removed and the mixture was stirred overnight at room temperature, TLC: toluene/ethyl acetate 8:2, R_f (**5**)=0.38. The solvent was evaporated under reduced pressure and the crude product, purified by flash column chromatography (SiO_2, eluent: toluene/ethyl acetate 95:5) and crystallized from hexanes giving aldehyde **5** (90 mg, 32% yield) M.p.=136–137°C; ^{1}H NMR (250 MHz, $CDCl_3$): δ=10.09 (s, 1H), 8.22 (d, 2H), 7.96 (m, 3H), 6.52 (m, 2H), 5.50 (s, 2H), 3.47 (quart, 4H), 3.02 (quart, 2H), 2.56 (s, 3H), 1.27 ppm (m, 9H); ^{13}C NMR (62.9 MHz, $CDCl_3$): δ=191.57, 178.22, 165.22, 152.18, 152.05, 149.97, 139.80, 139.27, 134.71, 130.37, 129.52, 124.12, 119.21, 110.45, 110.27, 59.30, 44.84, 25.55, 16.85, 15.45, 12.78 ppm; IR (KBr): $\tilde{\nu}$=3427, 2970, 1727, 1703, 1597, 1545, 1516, 1457, 1353, 1245, 1195, 1170, 1111, 1073, 1013, 932, 847, 759, 698 cm^{-1}; UV/Vis (CH_2Cl_2): $\lambda_{max}(\varepsilon)$=224.0 (11400), 254.4 (19090), 513.6 nm (28850 $mol^{-1}dm^3cm^{-1}$); elemental analysis calcd (%) for $C_{25}H_{28}N_4O_3S$ (464.58): C 64.63, H 6.07, N 12.06, S 6.90; found: C 64.79, H 5.98, N 11.51, S 6.96.

Acknowledgements

We thank M. Minghetti (ISOF) for technical support and MIUR (PRIN 2004035502, FIRB RBNE01P4JF and RBAU017S8R) for financial support.

[1] H. Spanggaard, F. C. Krebs, *Sol. Energy Mater. Sol. Cells* **2004**, *83*, 125–146.
[2] H. Hoppe, N. S. Sariciftci, *J. Mater. Res.* **2004**, *19*, 1924–1945.
[3] C. J. Brabec, N. S. Sariciftci, J. C. Hummelen, *Adv. Funct. Mater.* **2001**, *11*, 15–26.
[4] C. J. Brabec, *Sol. Energy Mater. Sol. Cells* **2004**, *83*, 273–292.

[5] a) Special issue on thin solid films and nano-structured materials for photovoltaics (E-MRS 2003 Spring Conference—Symposium D): *Thin Solid Films* **2004**, *451/452*, 1–669; b) Special issue on the development of organic and polymer photovoltaics: *Sol. Energy Mater. Sol. Cells* **2004**, *83*, 125–321.
[6] K. M. Coakley, M. D. McGehee, *Chem. Mater.* **2004**, *16*, 4533–4542.
[7] W. U. Huyhn, J. J. Dittmer, A. P. Alivisatos, *Science* **2002**, *295*, 2425–2427.
[8] L. Manna, D. J. Milliron, A. Meisel, E. C. Scher, A. P. Alivisatos, *Nat. Mater.* **2003**, *2*, 382–385.
[9] W. J. E. Beek, M. M. Wienk, R. A. J. Janssen, *Adv. Mater.* **2004**, *16*, 1009–1013.
[10] A. C. Arango, S. A. Carter, P. J. Brock, *Appl. Phys. Lett.* **1999**, *74*, 1698–1700.
[11] S. Morita, A. A. Zakhidov, K. Yoshino, *Solid State Commun.* **1992**, *82*, 249–252.
[12] G. Yu, J. Gao, J. C. Hummelen, F. Wudl, A. J. Heeger, *Science* **1995**, *270*, 1789–1791.
[13] J. J. M. Halls, C. A. Walsh, N. C. Greenham, E. A. Marseglia, R. H. Friend, S. C. Moratti, A. B. Holmes, *Nature* **1995**, *376*, 498–500.
[14] N. S. Sariciftci, L. Smilowitz, A. J. Heeger, F. Wudl, *Science* **1992**, *258*, 1474–1476.
[15] F. Padinger, R. S. Rittberger, N. S. Sariciftci, *Adv. Funct. Mater.* **2003**, *13*, 85–88.
[16] C. J. Brabec, S. E. Shaheen, C. Winder, N. S. Sariciftci, P. Denk, *Appl. Phys. Lett.* **2002**, *80*, 1288–1290.
[17] The photovoltaic effect, in an inorganic semiconductor device involves the production of free charges (electrons and holes) under illumination and their collection at the electrodes. In organic semiconductor materials, photo-absorption does not produce free charges, but a bound hole-electron pair (exciton) so that its dissociation is required. It has been found that efficient exciton dissociation in a bulk heterojunction architecture occurs when the D–A components are intimately mixed in the entire device volume, so that each D–A interface is within a distance less than the exciton diffusion length (approximately 10 nm).
[18] X. Yang, J. K. J. van Duren, M. T. Rispens, J. C. Hummelen, R. A. J. Janssen, M. A. J. Michels, J. Loos, *Adv. Mater.* **2004**, *16*, 802–806.
[19] A. Cravino, N. S. Sariciftci, *J. Mater. Chem.* **2002**, *12*, 1931–1943.
[20] A. Cravino, N. S. Sariciftci, *Nat. Mater.* **2003**, *2*, 360–361.
[21] J.-F. Nierengarten, *Sol. Energy Mater. Sol. Cells* **2004**, *83*, 187–199.
[22] D. M. Guldi, C. Luo, A. Swartz, R. Gomez, J. L. Segura, N. Martin, C. J. Brabec, N. S. Sariciftci, *J. Org. Chem.* **2002**, *67*, 1141–1152.
[23] M. A. Loi, P. Denk, H. Hoppe, H. Neugebauer, C. Winder, D. Meissner, D. Brabec, N. S. Sariciftci, A. Gouloumis, P. Vazquez, T. Torres, *J. Mater. Chem.* **2003**, *13*, 700–704.
[24] J.-F. Eckert, J.-F. Nicoud, J.-F. Nierengarten, S.-G. Liu, L. Echegoyen, F. Barigelletti, N. Armaroli, L. Ouali, H. Krasnikov, *J. Am. Chem. Soc.* **2000**, *122*, 7467–7479.
[25] I. B. Martini, T. Da Ros, R. Helgeson, F. Wudl, B. J. Schwartz, *Chem. Phys. Lett.* **2000**, *327*, 253–262.
[26] M. Maggini, G. Possamai, E. Menna, G. Scorrano, N. Camaioni, G. Ridolfi, G. Casalbore-Miceli, L. Franco, M. Ruzzi, C. Corvaja, *Chem. Commun.* **2002**, 2028–2029.
[27] S. Cattarin, P. Ceroni, D. M. Guldi, M. Maggini, E. Menna, F. Paolucci, S. Roffia, G. Scorrano, *J. Mater. Chem.* **1999**, *9*, 2743–2750.
[28] M. Prato, M. Maggini, *Acc. Chem. Res.* **1998**, *31*, 519–526.
[29] T. Da Ros, M. Prato, F. Novello, M. Maggini, E. Banfi, *J. Org. Chem.* **1996**, *61*, 9070–9072.
[30] M. Maggini, G. Scorrano, M. Prato, *J. Am. Chem. Soc.* **1993**, *115*, 9798–9799.
[31] The absorption spectra of dyads **2b**–**4b** is not exactly the sum of the absorptions of the dye and fullerene moieties. In fact, a red-shift of the visible band was noted, as reported and discussed earlier for dyad **1b** in the paper cited in ref. [30].
[32] D. M. Guldi, M. Prato, *Acc. Chem. Res.* **2000**, *33*, 695–703.
[33] The yields were determined through the comparative method. In particular, the extinction coefficients of the triplet–triplet and the fullerene radical anion with values of $\varepsilon_{700nm}=16100\,M^{-1}cm^{-1}$ and $\varepsilon_{1000nm}=4700\,M^{-1}cm^{-1}$, respectively, were considered. a) C. Luo, M. Fujitsuka, A. Watanabe, O. Ito, L. Gan, Y. Huang, C.-H. Huang, *J. Chem. Soc. Faraday Trans.* **1998**, *94*, 527–532; b) C. Luo, M. Fujitsuka, C.-H. Huang, O. Ito, *Phys. Chem. Chem. Phys.* **1999**, *1*, 2923–2928.
[34] G. Agostini, C. Corvaja, L. Pasimeni, *Chem. Phys.* **1996**, *202*, 349–356.
[35] M. A. El-Sayed, D. S. Tinti, E. M. Yee, *J. Chem. Phys.* **1969**, *51*, 5271–5273.
[36] K. Akiyama, S. Tero-Kubota, *Mol. Phys.* **1994**, *83*, 1091–1097.
[37] K. Akiyama, S. Tero-Kubota, T. Ikoma, Y. Ikegami, *J. Am. Chem. Soc.* **1994**, *116*, 5324–5327.
[38] S. Ceola, C. Corvaja, L. Franco, *Mol. Cryst. Liq. Cryst.* **2003**, *391*, 31–43.
[39] A. Zoleo, A. L. Maniero, M. Prato, M. G. Severin, L. C. Brunel, K. Kordatos, M. Brustolon, *J. Phys. Chem. A* **2000**, *104*, 9853–9863.
[40] C. J. Brabec, A. Cravino, D. Meissner, N. S. Sariciftci, T. Fromherz, M. T. Rispens, L. Sanchez, J. C. Hummelen, *Adv. Funct. Mater.* **2001**, *11*, 374–380.
[41] H. Peeters, P. A. van Hal, J. Knol, C. J. Brabec, N. S. Sariciftci, J. C. Hummelen, R. A. J. Janssen, *J. Phys. Chem. B* **2000**, *104*, 10174–10190.
[42] A. M. Ramos, M. T. Rispens, J. K. J. van Duren, J. C. Hummelen, R. A. J. Janssen, *J. Am. Chem. Soc.* **2001**, *123*, 6714–6715.
[43] J.-F. Nierengarten, T. Gu, T. Aernouts, W. Geens, J. Poortmans, G. Hadziioannou, D. Tsamouras, *Appl. Phys. A* **2004**, *79*, 47–49.
[44] G. Possamai, N. Camaioni, G. Ridolfi, L. Franco, M. Ruzzi, E. Menna, G. Casalbore-Miceli, A. M. Fichera, G. Scorrano, C. Corvaja, M. Maggini, *Synth. Met.* **2003**, *139*, 585–588.
[45] J. K. J. van Duren, X. Yang, J. Loos, C. W. T. Bulle-Lieuwma, A. B. Sieval, J. C. Hummelen, R. A. J. Janssen, *Adv. Funct. Mater.* **2004**, *14*, 425–434.
[46] P. Samorì, J. P. Rabe, *J. Phys. Condens. Matter* **2002**, *14*, 9955–9973.
[47] A. Bianco, M. Maggini, G. Scorrano, C. Toniolo, G. Marconi, C. Villani, M. Prato, *J. Am. Chem. Soc.* **1996**, *118*, 4072–4080.
[48] G. Hansen, E. Schefczik, H.-H. Etzbach, H. Reichelt, H. Loeffler (to BASF-DE), EP0201896 (12/05/1986).

Received: January 19, 2005
Revised: May 9, 2005
Published online: July 25, 2005

